LARGE EDDY SIMULATION OF ENCLOSED ROTOR-STATOR FLOW

W. Lo, C. W. Chen and C. A. Lin
Department of Power Mechanical Engineering,
National Tsing Hua University
Hsinchu 30013, Taiwan
calin@pme.nthu.edu.tw

ABSTRACT

Large eddy simulation is applied to simulate the turbulent flows within rotor-stator cavity. Parallel computation is achieved using the domain decomposition and SPMD model. For the rotor-stator flow, the internal structure is induced by the diffusive transport of the tangential momentum from the rotor into the interior. The instantaneous azimuthal vorticity contours near the stator and rotor show stretching and elongated structure in the tangential direction. Near the rotor, the vorticity line is more coherent; however along its counterpart location at the stator wall, the structure is more chaotic. This shows that the turbulence intensity along the stator wall is much more enhanced compared to that on the rotor wall. A laminar region is also identified near the shaft at small radii. Capability of the adopted LES model is also examined by comparing the predicted flow quantities with available measured data.

INTRODUCTION

The enclosed rotor-stator case, where no external through flow is present across the disk boundary, is rather complex. The internal flow field is induced by the diffusive transport of tangential momentum from the rotor wall into the cavity interior. Therefore, the thin boundary layer, (the Ekman layer), on the wall exerts significant influence on the momentum transport and also heat transfer, and hence intense interaction of wall and the internal flow fields exist. Two distinct features characterize the flow field. The first one is the single circulating vortex caused by the imbalance of centrifugal forces which produce the radial outflow over the rotor side and a radial inflow over the stator side; and the second is the gradual transition from laminar to turbulent flow when the flow travels to large radii. An inviscid core exists between the two thin boundary layers that the radial velocity is virtually zero. Comprehensive discussions of the rotating disk cavity flows can be found in Owen and Rogers (1989).

Despite its geometric simplicity, numerical predictions of the enclosed rotor-stator flow fields, for example, are restrained by various obstacles, such as the numerical accuracy and the representation of turbulence (Morse, 1991; Iacovides and Theofanopoulos, 1991). The effects of the moving wall or rotation on the turbulence field and the possible coexistence of laminar and turbulent regions make it a difficult task. The measurements of Itoh et al.(1990) also indicated that the turbulence on the rotor side is severely damped under to that on the stator side. However, few of the previous proposed models are capable of reproducing the complex flow characteristics in the rotor-stator system.

It is generally accepted that the Coriolis force can considerably affect turbulent flows. Traditionally, these effects are investigated by studying parallel shear flows under orthogonal mode rotation, i.e. when the axis of rotation is either parallel or antiparallel to the mean flow vorticity vector. Turbulence is usually suppressed if the rotation vector is parallel to the vorticity vector, and enhanced if they are antiparallel. This is similar to the stabilizing and destabilizing effects for a shear flow entering a convex and a concave curvature. So, it was suggested that the Reynolds stress transport model is needed to deal with the complex flows present in rotating cavity flows.

However, Computations of Elena and Schiestel (1995) indicated that though the Reynolds stress transport model (Hanjalic and Launder, 1976) performs better at the stator side, its performance at the rotor side is surprisingly similar to the $k-\epsilon$ model(Launder and Sharma, 1974). Both models show reduced levels of diffusion at the rotor side. Therefore, the capability of the inherent interaction of swirl and turbulence present in the RSTM model does not seem to play a major role. There may be another mechanism which is absent in the models. Elena and Schiestel (1996) further improved their results by adding rotation and local vorticity sensitized empirical terms in the k equation. The effect of this term is to increase the turbulence level at the rotor side. It was argued that these are to model the effect of the pressure diffusion process at this region, which is absent in the model of Hanjalic and Launder. Therefore, this seems to suggest that the accurate near wall modeling is important in the present rotor-stator geometry.

Hwang and Lin (2003) examined the influence of rotation on the flow field and turbulence modeling by sensitizing the turbulence model coefficient to rotational Richardson number, and the effect was found to be marginal. By adopting an improved low Reynolds number $k-\epsilon$ model (Hwang and Lin, 1998), the model reproduces correctly the gradual thickening of the Ekman layers from small to large radii, which is due to the transition from laminar to turbulent regimes, especially on the rotor side within the disk cavities. The elevated level of turbulence on the stator side compared to that on the rotor side is also predicted correctly by the model. However, the level of diffusive transport on the stator side was still under-predicted.

In the present study, the large eddy simulation technique is adopted to predict the flows within the enclosed rotor-stator. Focuses will be on the predicting capability of the LES model to internal flow fields and the differential levels of turbulence on the stator and rotor walls. Since the LES requires the solutions of three-dimensional time dependent equations, and this requires the usage of parallel computers. Therefore, the implementation of parallel algorithm and its efficiency are also addressed.

GOVERNING EQUATIONS AND MODELING

LES is based on the definition of a filtering operation: a

filtered (or resolved, or large-scale) variable is defined as,

$$f(\tilde{x}) = \int_D f(\tilde{x'})G(\tilde{x},\tilde{x'})d\tilde{x'} \quad (1)$$

where D is the entire domain and G is the filter function. The filter function determines the size and structure of the small scales.

The governing equations are grid-filtered, incompressible continuity and Navier-Stokes equations (in cartesian tensor form),

$$\frac{\partial \rho \overline{u}_i}{\partial x_i} = 0 \quad (2)$$

$$\frac{\partial \rho \overline{u}_i}{\partial t} + \frac{\partial}{\partial x_j}(\rho \overline{u}_i \overline{u}_j) = -\frac{\partial \overline{p}}{\partial x_i} + \frac{\partial}{\partial x_j}[\mu(\frac{\partial \overline{u}_i}{\partial x_j} + \frac{\partial \overline{u}_j}{\partial x_i}) - \tau_{ij}] \quad (3)$$

where

$$\tau_{ij} = \rho\overline{u_i u_j} - \rho\overline{u}_i\overline{u}_j$$

is the sub-grid stress due to the effects of velocities being not resolved by the computational grids.

In the present study, the Smagorinsky model (Smagorinsky, 1963) has been used for the sub-grid stress, such that,

$$\tau_{ij} = -\rho(C_s\Delta)^2 \frac{1}{\sqrt{2}}\sqrt{S_{kl}S_{kl}}S_{ij} + \frac{2}{3}\rho k_{sgs}\delta_{ij} \quad (4)$$

where $C_s = 0.1$, $S_{ij} = \frac{\partial \overline{u}_i}{\partial x_j} + \frac{\partial \overline{u}_j}{\partial x_i}$ and $\Delta = (\Delta x \Delta y \Delta z)^{1/3}$, respectively. It can be seen that in the present study the mesh size is used as the filtering operator.

A Van Driest damping function accounts for the effect of the wall on the subgrid-scale is adopted here and takes the form as,

$$l_m = \kappa y[1 - exp(-\frac{y^+}{25})] \quad (5)$$

where y is the distance to the wall and the cell size is redefined as,

$$\Delta = MIN[l_m, (\Delta x \Delta y \Delta z)^{1/3}] \quad (6)$$

NUMERICAL ALGORITHMS

All the spatial derivative are discretised using second-order central differencing scheme within the staggered finite volume arrangement. The time integration method adopted for the transport equation is based on the semi-implicit, fractional step method. A four step time advancement scheme (Choi and Moin 1994) is adopted, i.e.,

$$\frac{\overline{u}_i^* - \overline{u}_i^n}{\Delta t} + \frac{3}{2}C_i^n - \frac{1}{2}C_i^{n-1} = -\frac{\partial p^n}{\partial x_i}$$
$$+\frac{3}{2}D_{i,p}^n - \frac{1}{2}D_{i,p}^{n-1} + \frac{1}{2}(D_{i,n}^* + D_{i,n}^n) \quad (7)$$

$$\frac{\overline{u}_i^{**} - \overline{u}_i^*}{\Delta t} = \frac{\partial p^n}{\partial x_i} \quad (8)$$

$$\frac{\partial}{\partial x_i}\frac{\partial p^{n+1}}{\partial x_i} = \frac{1}{\Delta t}\frac{\partial \overline{u}_i^{**}}{\partial x_i} \quad (9)$$

$$\frac{\overline{u}_i^{n+1} - \overline{u}_i^{**}}{\Delta t} = -\frac{\partial p^{n+1}}{\partial x_i} \quad (10)$$

where C_i are the convective fluxes and $D_{i,p}$ and $D_{i,n}$ are diffusive fluxes in the wall parallel and normal directions, respectively.

Therefore, it can be seen that the explicit and implicit terms are advanced using the Adams-Bashforth and Crank-Nicholson methods, respectively. The discretised algebraic equations are solved by application of the CGSTAB solver (Van den Vorst and Sonneveld, 1990).

The continuity is satisfied through the solution of a Poisson equation (equation 9). The Poisson equation for pressure is solved using a combination of Fourier transform and the CGSTAB method. Because the grid spacing is uniform in the tangential direction, together with the adoption of the periodic boundary conditions, Fourier transform can be used to reduce the 3-D Poisson equation to uncoupled 2-D algebraic equations.

Because the above numerical framework is explicit in the tangential direction, the adopted scheme can be parallelized using the domain decomposition and the single program multiple data (SPMD) model. Each processor has direct access to its local memory, however the information sharing between processors and the reference to non-local memory have to go through the interconnection networks via message-passing MPI. The 3D grid is partitioned among processors. Data in the tangential direction are distributed among processors while the dimensions along the axial and radial directions are not distributed. The data distribution is [*,*,Block], where "Block" distribution assigns a contiguous block of array elements to each processor and "*" means no distribution in that dimension.

One drawback of the above parallel implementation is that excessive data movement among processors is required when applying the Fourier transform in solving the Poisson equation in the tangential direction.

The platforms of the parallel computations are IBM P690 and PC cluster. For IBM P690, there are 8 nodes and each node has 32 cpus. As for PC cluster, there are 32 dual cpu nodes with Myrinet. For IBM P690, each node has 32 cpus with a shared memory, which is beneficial for cross cpu data transfer due to Fourier transform. The parallel efficiency using IBM P690 is shown in Figure 1. It can be clearly observed that the problem size has a drastic effect on the parallel efficiency, where a higher level of efficiency is achieved with the elevated level of problem size. Super-linear speed-up is also observed for the 120x120x80 grid and this phenomenon is particularly pronounced using IBM P690 machine. This is partly due to the use of cache at multiple-cpu runs.

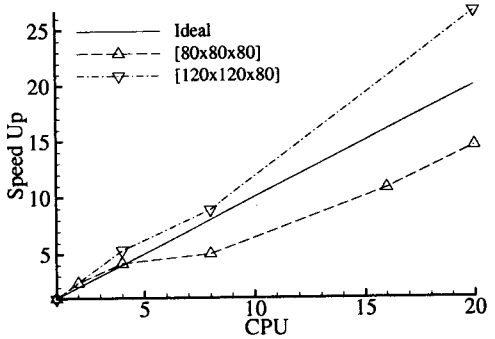

Figure 1: Parallel efficiency

RESULTS

Figure 2 shows the geometry of the enclosed disk cavity, where the moving parts (rotors:rotating shaft and disk) are rotating at an angular velocity of Ω. The mesh sizes adopted are 120x120x80 and 80x80x80 in the axial, radial and tangential directions, respectively. Preliminary results

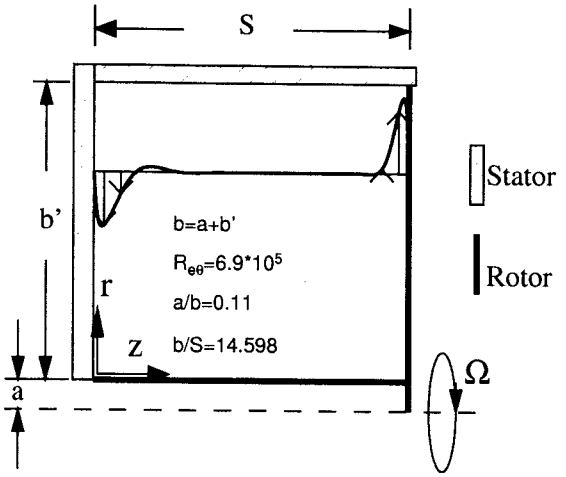

Figure 2: Geometry of Daily et al.

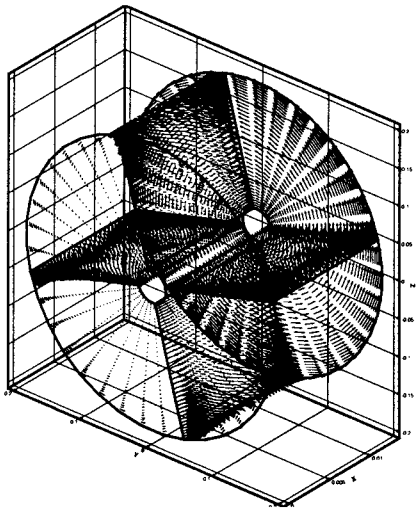

Figure 3: Instantaneous velocity vector plot

show marginal difference between the two grids. Therefore, in subsequent discussions the 80x80x80 grid will be used. In the tangential direction, the computational domain is 2π and with a uniform mesh, which allows for the implementation of the periodic boundary condition and Fourier transform. In the radial and axial directions, the mesh is clustered near the wall using the tanh function.

Since the disk cavity is enclosed, no inlet boundary condition is needed. No slip and impermeable wall conditions are applied, except along the rotor walls, where the rotor tangential velocity is prescribed according to the angular velocity. Predictions focus on case in which the rotational Reynolds number ($Re_\theta = \Omega b^2/\nu$) is 6.9×10^5. The predicted results will be contrasted with measurements by Daily et al. (1964).

Figure 3 shows the instantaneous velocity vector plot within the disk cavity. The elevated level of tangential velocity along the rotating wall can be clearly observed. The secondary flow can also be seen from the cross sectional views at four selected locations. The instantaneous azimuthal vorticity contours near the stator and rotor are shown in Figures 4 and 5. The stretching of the vorticity can be observed by the elongated contours. At location Z/S=0.992, the vorticity line is more coherent; however along its counterpart location at the stator wall, the structure is more chaotic. As will be shown later, the turbulence intensity along the stator wall is much more enhanced compared to that on the rotor wall. At small radii near the shaft, the vorticity level is reduced. As a rule of thumb, the flow remains laminar at $R_{e\theta} < 10^5$, which corresponds to location at $r/b = 0.15$.

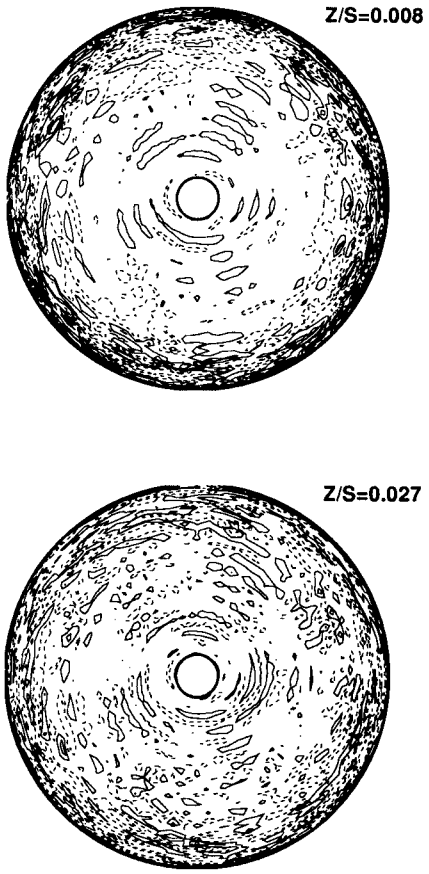

Figure 4: Instantaneous azimuthal vorticity field-stator side (solid line: positive; dotted line: negative)

Responses to the turbulence representation are best exemplified by observing the variations of the radial velocity (V_r) and tangential velocity (V_θ), shown in Figures 6 and 7. It is apparent that outside the thin Ekman layers the fluid possesses no radial component, as shown in Figure 6. The measurements indicate that the radial velocity is maximum on the rotor side, due to the lower level of turbulence present in this region. The present LES model correctly captures this phenomenon, although there is a discrepancy on the rotor and stator sides in the region $r/b > 0.6$, where the model predicts a slightly reduced level of diffusive transport across the Ekman layers.

The tangential velocity, shown in Figure 7, is seen to remain uniform in the core region and varies steeply across the thin near-wall regions. At $r/b = 0.47$, shown in Figure 7 (a), the level of the diffusive transport predicted by the LES model is further supported by the measurements. At $r/b = 0.65$, the model predicts a slightly lower tangential velocity in the core region than is indicated by the measurements. In the region $r/b = 0.83$, comparisons with measurements indicate that the LES shows a correct tangential velocity.

For comparison purposes, $k-\epsilon$ predictions of Hwang and Lin (2003) and laminar solutions are also included. Details

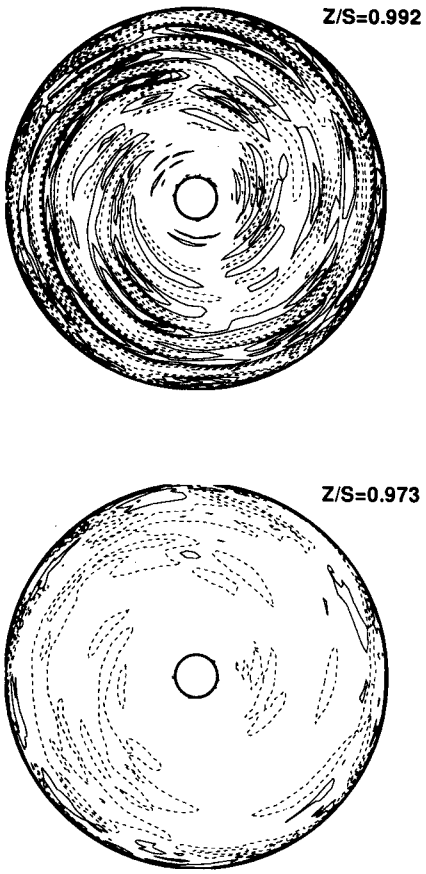

Figure 5: Instantaneous azimuthal vorticity field-rotor side (solid line: positive; dotted line: negative)

of the $k-\tilde{\epsilon}$ model can found in Hwang and Lin (1998). It can be seen that the performance of both the LES and H-L $k-\tilde{\epsilon}$ are similar, though the results of LES are marginally better. The radial velocity profiles on the stator wall are significantly different between the turbulent and laminar solutions. However, the radial profiles on the rotor walls show similar results, which indicates that the turbulence level on the rotor is low. On the other hand, this also implies that the turbulence level on the stator wall is enhanced.

Figure 8 shows polar plots of the velocity distributions. $V_{\theta rc}$ is the tangential velocity at the mid plane z/b=0.5. The predicted data location is at r/b=0.83, while the measured data location is at r/b=0.6. These correspond to the location-Rotational Reynolds number ($Re_L = \Omega r^2/\nu$) being 4.8×10^5 and 3.6×10^5, respectively. Reasonable agreements are achieved, though the measurements of Itoh et al. (1990) were conducted at $Re_\theta = 10^6$ and without the presence of central shaft.

Figure 9 shows the distributions of the turbulence kinetic energy at three radial locations. It can be clearly seen that the turbulence level on the stator wall is higher than that on the rotor wall. This confirms the finding of Itoh et al. (1990) where the turbulence on the rotor side is severely damped under to that on the stator side, and is also consistent with the predicted mean flow fields. Also, the turbulence level increases in tandem with the radius.

The distributions of the LES predicted Reynolds stresses

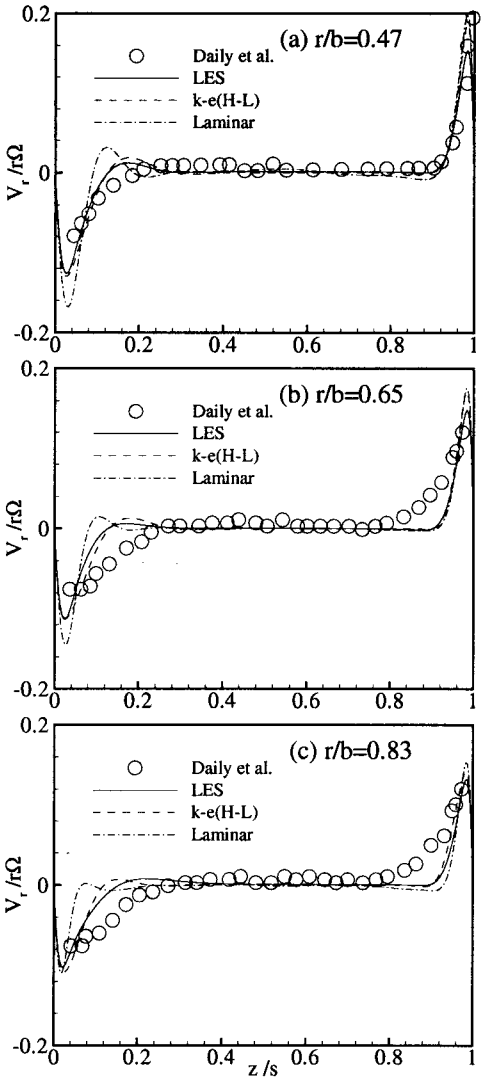

Figure 6: Radial velocity

are shown in Figures 10 to 11 at three radial locations. Again, turbulence levels on the stator wall (z/s=0) are in general higher than that on the rotor wall (z/s=1). As is expected, the turbulence intensity along the tangential direction is the highest. The lower levels of shear stresses $\overline{v'_\theta v'_z}$ and $\overline{v'_z v'_r}$ are the causes of the thin Ekman layers along the rotor wall.

CONCLUSION

Large eddy simulation is applied to simulate the turbulent flows within rotor-stator cavity. Parallel efficiency using the domain decomposition and SPMD model is good. For rotor-stator flow, the internal structure is induced by the diffusive transport of the tangential momentum from the rotor into the interior. The instantaneous azimuthal vorticity contours near the stator and rotor show stretching and elongated structure in the tangential direction. Near the rotor, the vorticity line is more coherent; however along its counterpart location at the stator wall, the structure is more chaotic. This shows that the turbulence intensity along the stator wall is much more enhanced compared to that on the rotor wall. Therefore, the predicted thickness of the Ekman layer is found to be thinner on the rotor side. Turbulence

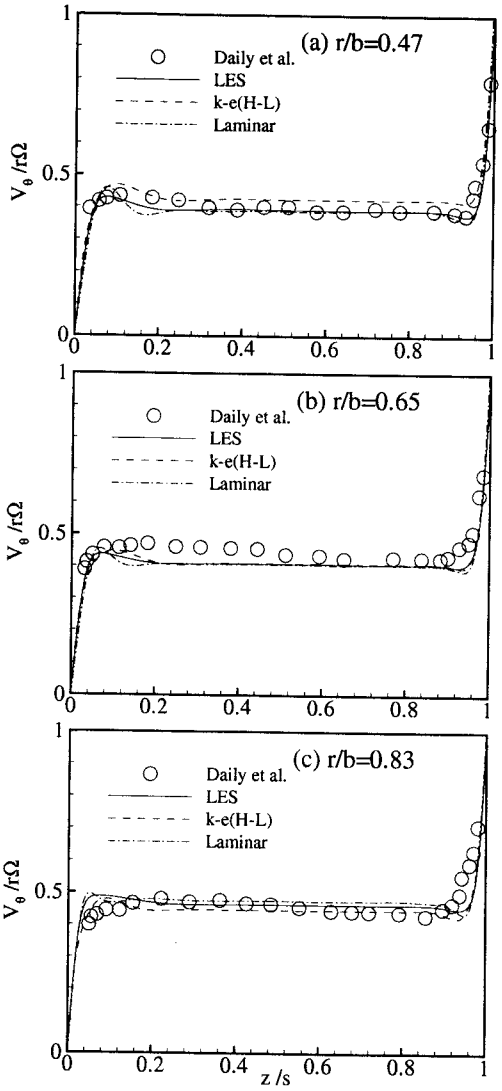

Figure 7: Tangential velocity

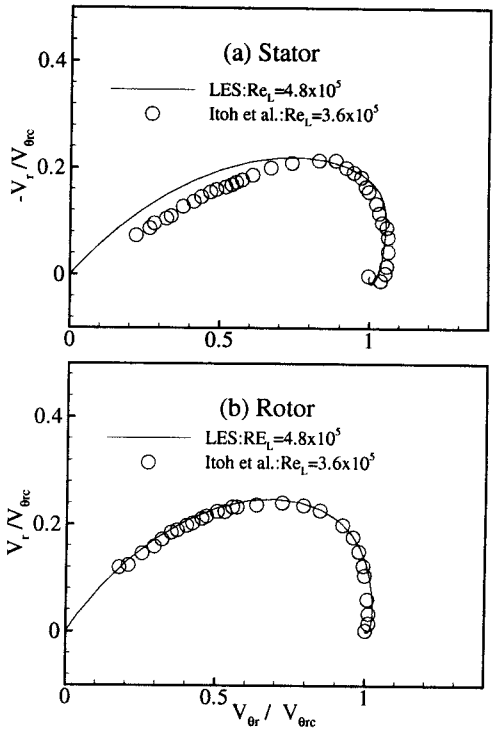

Figure 8: Polar plots of velocity distributions

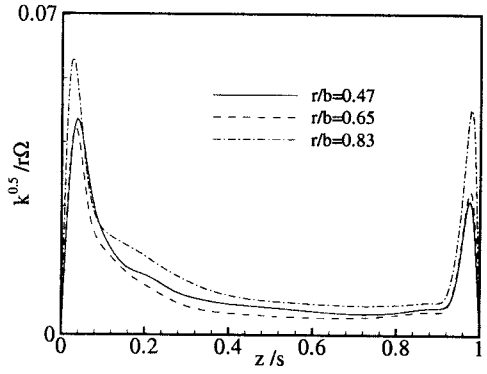

Figure 9: Turbulence kinetic energy

level also increases in tandem with the radius. A laminar region is also identified near the shaft at small radii. The LES model correctly reproduces the differential turbulence levels between the rotor and stator. However, comparisons with the measured data indicate that the LES model predicts reduced level of the diffusive transport across the Ekman layers at large radii of the disk cavity.

ACKNOWLEDGMENTS

This research work is supported by the National Science Council of Taiwan under grant 90-2212-E-007-058 and the computational facilities are provided by the National Centre for High-Performance Computing of Taiwan which the authors gratefully acknowledge.

REFERENCES

Choi, H. and Moin, P. A., "Effects of the Computational Time Step on Numerical Solutions of Turbulent Flow," Journal of Computational Physics, Vol. 113, 1994, pp. 1-4.

Daily, J.W., Ernst, W.D. and Asbedian, V.V., "Enclosed rotating disks with superposed through-flows:mean steady and periodic unsteady characteristics of induced flow, " Report No.64, Hydrodynamic Lab., Massachusetts Institute of Technology, 1964.

Elena, L. and Schiestel, R., "Turbulence Modeling of Confined Flow in Rotating Disk System," AIAA Journal, Vol. 33, No. 5, 1995, pp. 812-821.

Elena, L. and Schiestel, R., "Turbulence modeling of rotating confined flows," International Journal of Heat and Fluid Flow, Vol. 17, No. 3, 1996, pp. 283-289.

Hanjalic, K. and Launder, B. E., "Contribution towards a Reynolds-stress closure for low-Reynolds number turbulence," Journal of Fluid Mechanics, Vol. 74, 1976, pp. 583-610.

Hwang, C. B. and Lin, C. A., "Improved low-Reynolds-number $k-\widetilde{\varepsilon}$ model based on direct numerical simulation data," AIAA Journal, Vol. 36, No.1, 1998, pp. 38-43.

Hwang, C. B. and Lin, C. A., "Low-Reynolds-Number k-$\tilde{\epsilon}$ Modeling of Nonstationary Solid Boundary Flows," AIAA Journal, Vol. 41, No.2, 2003, pp. 168-175.

Iacovides, H. and Theofanopoulos, I. P., "Turbulence modeling of axisymmetric flow inside rotating cavities," International Journal of Heat and Fluid Flow, Vol. 12, No. 1, 1991, pp. 2-11.

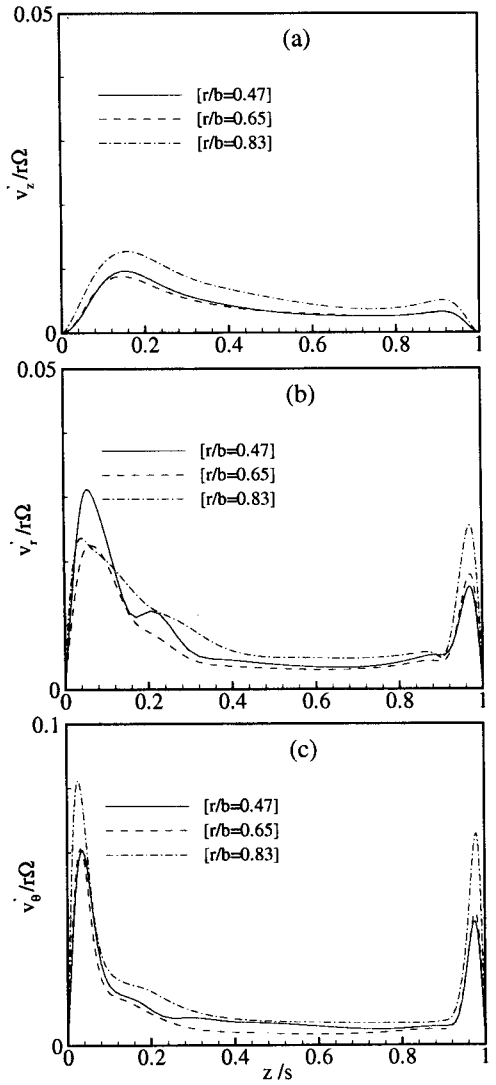

Figure 10: Turbulence intensity

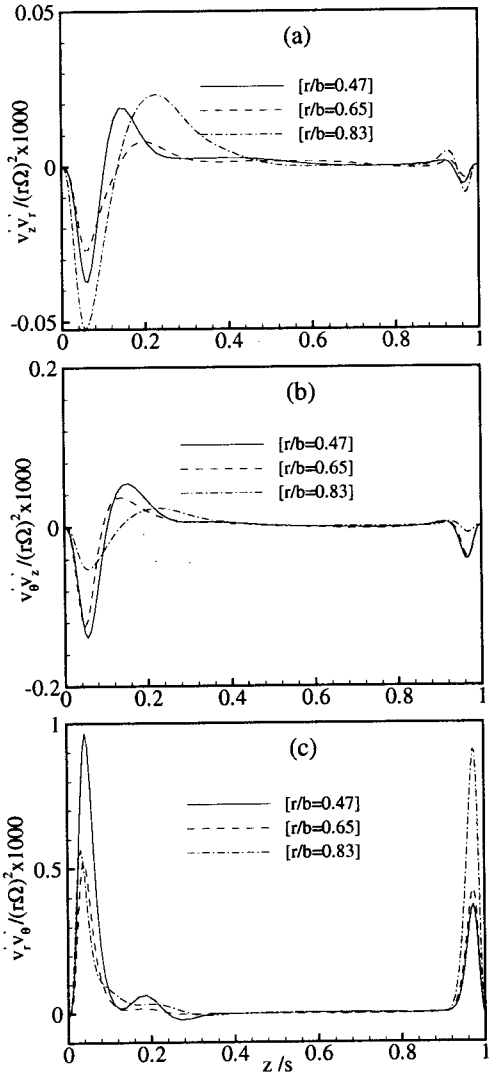

Figure 11: Shear stresses

Itoh, M., Yamada, Y., Imao, S. and Gouda, M., "Experiment on turbulent flow due to an enclosed rotating disc," Proceeding of 1st Symposium on Engineering Turbulence Modeling and Experiments, Dubrovnik, Yugoslavia, 1990, pp. 659-668.

Launder, B. E., and Sharma, B. I., "Application of the Energy Dissipation Model of Turbulence to the Calculation of Flow Near a Spinning Disc," Letters in Heat and Mass Transfer, Vol. 1, No. 2, 1974, p. 131-138.

Morse, A. P., "Assessment of laminar-turbulent transition in closed disk geometries," ASME Journal of Turbomachinery, Vol. 113, No. 1, 1991, pp. 131-138.

Owen, J. M. and Rogers, R. H., "Flow and heat transfer in rotating-disc systems," Vol. I, Rotor-Stator Systems, Wiley, New York, 1989.

Smagorinsky, J., 1963, "General Circulation Experiments with the Primitive Equations. I. The Basic Experiments," Monthly Weather Review, Vol. 91, pp. 99-164.

Van den Vorst, H. A. and Sonneveld, P., " CGSTAB, a more smoothly converging variant of CGS," Technical Report 90-50, Delft University of Technology, 1990.